Final Report

Project Title: Development & Optimization of Materials and Processes for a Cost Effective Photoelectrochemical Hydrogen Production System

Project Period: October 1, 2006 to May 31, 2008 NCE to May 31, 2010
Date of Report: November 1, 2010
Recipient: University of California Santa Barbara
Working Partners: NREL
Award Number: DE-FG36-05GO15040
Cost-Sharing Partners: University of California Santa Barbara

Contact: Eric W. McFarland
Dept. of Chemical Engineering
University of California
Santa Barbara, CA 93106-5080
Phone: 805-893-4343
Fax: 805-893-4731
mcfar@engineering.ucsb.edu

DOE Managers: Roxanne Garland, DOE Office of Energy Efficiency and Renewable Energy

Executive Summary:

The overall project objective was to apply high throughput experimentation and combinatorial methods together with novel syntheses to discover and optimize efficient, practical, and economically sustainable materials for photoelectrochemical production of bulk hydrogen from water. Automated electrochemical synthesis and photoelectrochemical screening systems were designed and constructed and used to study a variety of new photoelectrocatalytic materials. We evaluated photocatalytic performance in the dark and under illumination with or without applied bias in a high-throughput manner and did detailed evaluation on many materials. Significant attention was given to α-Fe_2O_3 based semiconductor materials and thin films with different dopants were synthesized by co-electrodeposition techniques. Approximately 30 dopants including Al, Zn, Cu, Ni, Co, Cr, Mo, Ti, Pt, etc. were investigated. Hematite thin films doped with Al, Ti, Pt, Cr, and Mo exhibited significant improvements in efficiency for photoelectrochemical water splitting compared with undoped hematite. In several cases we collaborated with theorists who used density functional theory to help explain performance trends and suggest new materials. The best materials were investigated in detail by X-ray diffraction (XRD), scanning electron microscopy (SEM), ultraviolet-visual spectroscopy (UV-Vis), X-ray photoelectron spectroscopy (XPS). The photoelectrocatalytic performance of the thin films was evaluated and their incident photon

conversion efficiency (IPCE) determined. The underlying mechanism for the improved photoelectrocatalytic (PEC) performance from doping was explored. The significant increases in performance for Cr or Mo doped hematite thin films is attributed to an improvement in the charge transport properties within the films and not due to significant changes in the electrocatalytic rates due to dopants residing at the surface. Pt acts as an electron donor (substitution of a Fe^{3+} by Pt^{4+}) in the hematite lattice and the increased donor concentration of the n-type semiconductor is responsible for the improved performance. In Al doped hematite films, theory helped us to understand that the improvements are due to the increased conductivity of the hematite associated with the strain introduced in the lattice from Al substitution of Fe. We also developed a means to shift the conduction band position using fluorine surface modification of Ti doped hematite. We were also able to explore novel metal oxide semiconductors of the delafossite class, $Cu(X)O_2$ (X = Cr, La, Ga). In general, we have found that the oxides under investigation in this project can be considerably improved in terms of efficiency, however, we are not optimistic that any oxide material will have sufficient solar-to-chemical efficiency to meet the DOE targets or be suitable for cost effective hydrogen production. Given our conclusion that the known metal oxides can not meet realistic performance criteria for solar-to-chemical conversion efficiency, we have recently moved all our efforts to metal phosphide semiconductors. Beginning with commercially available InP wafers we investigated stability of InP in a variety of electrolytes. Sulfur surface treatment and surface deposition of Pt group metal nanoparticles were demonstrated to improve InP stability then later similar effects were shown on tungsten phosphide, WP, powders. Sulfur treatment also significantly improves hydrogen production in WP. A simple two-step route was developed to synthesize several transition metal phosphides (MoP, WP, Ni_2P, FeP) and doped gallium phosphides (GaM)P (e.g., M = Mo). This synthesis method has the potential for high throughput synthesis. Our work, together with process engineering colleagues, has shown that the only likely commercial process implementation will be in slurry-type reactors and we have begun testing and screening new materials in slurry format to show the viability of this approach. We have developed specific schemes for minimizing the back-reactions which are a feature of slurry based systems.

Overall, the project succeeded in the following areas: i) application of high-throughput and combinatorial chemistry methods to the investigation and discovery of new photoelectrochemical material systems, ii) we showed how the combination of theory and experiment can be effectively used to optimize metal oxide semiconductors, iii) through our work with engineering system colleagues identifying performance criteria it has become clear that the metal oxides we and others have explored as photoelectrode systems will not be cost-effective and significant improvements can only be achieved in new (non-metal oxide) classes of materials and an exploration of phosphides has been initiated. We are gratified that this DOE sponsored research has provided support for the education of many young scientists whose training made possible by this project will benefit the US taxpayers far into the future.

Project Achievements vs. Objectives:

The major objectives as listed in the proposal were: 1) Discovering and optimizing the composition of a potential photocatalytic material, 2) Optimizing the nanostructure of the material for maximum efficiency, and 3) Creating a conceptual large-scale reactor design in which the material might realistically be used for producing hydrogen. The specific achievements towards each objective are summarized below:

1) Discovery and optimization of potential photocatalytic materials

Developed high-throughput methods for synthesis and screening of new photocatalytic materials and deployed the new instrumentation hardware for investigations of hematite. Substitutional doping improved the electronic properties of α-Fe_2O_3, generally speaking, nonisovalent substitutional doping enhanced the electronic conductivity of α-Fe_2O_3. Co-deposition with Cr or Mo in hematite in varying compositions of Cr and Mo created active photoanodes for photoelectrochemical water splitting. The best performing samples were 5% Cr and 15% Mo doped which had Incident Photon Conversion Efficiencies (IPCE's) at 400 nm of 6% and 12%, respectively, with an applied potential of 0.4 V vs Ag/AgCl. Pt-doped α-Fe_2O_3 thin films were active for photoelectrochemical water splitting. We also found that introduction of strain by isovalent substitutional doping with Al improved the electronic conductivity. We developed a microwave plasma reactor and reaction conditions for the synthesis of amorphous SiC nanoparticles in a continuous gas phase process are amenable to large scale production use. The process utilizes the decomposition of tetramethylsilane (TMS) for both the silicon and the carbon source. PEC performance of the materials was poor and oxidation in electrolyte irreversible and destructive. Our most recent work has focused on phosphide based materials and in better understanding their stability, photocorrosion in the electrolytes, and means of synthesis in a high throughput manner. A simple two-step route was developed to synthesize several transition metal phosphides (MoP, WP, Ni_2P, FeP) and doped gallium phosphides (GaM)P (e.g., M = Mo). This synthesis method has the potential for high through-put synthesis. Further optimizations were performed on hematite films and CoF3 aqueous solution was used to modify the surface of doped iron oxide thin film photoanodes to negatively shift the flat-band potential and allow photogenerated electrons to directly reduce water to hydrogen without an external bias.

2) Optimizing the nanostructure of the material for maximum efficiency

Our objective was to develop combinations of absorbers and electrocatalysts which provided efficient transfer of photogenerated electrons and holes to produce hydrogen and oxygen. A three-step method was employed to synthesize monodispersed silica encapsulated composite nanostructures with Pt nanoclusters (<1 nm) densely deposited on the surface of core hematite nanocubes. In addition, we developed nanocomposite magnetite cores with silica shells. Electrocatalytic metals were produced including gold-platinum (Au-Pt) clusters synthesized by electrodeposition. A nickel iron binary oxide electrocatalysts prepared from different precursors were evaluated to facilitate the oxygen evolution reaction (OER) on

photoelectrodes and their activities characterized. The kinetics of electrocatalytic oxygen reduction in basic electrolyte on Au nanoparticles was also determined for 3 and 7 nm clusters supported on carbon. Finally, the electroreduction of oxygen was investigated on mixed gold-cobalt oxide (Au/CoO_x) nanoclusters in potassium hydroxide solution. The Au/CoO_x binary electrocatalysts with less than 1.2% Co atoms were found to increase the ORR activity compared to those of either the pure Au or pure CoO_x.

3) Create a conceptual large-scale reactor system in which a PEC material might realistically be used for producing hydrogen

In collaboration with colleagues at Directed Technologies we participated in the development of a photoelectrochemical process economic model which showed that the most promising system design for cost effective hydrogen production is based on a slurry phase reactor design. We extended this model to examine a process for the conversion of organic wastewater associated with biofuel production as a source of oxidation potential for hydrogen production. Preliminary studies showed that significantly improved conversion efficiencies for hydrogen production were possible even for metal oxides (hematite) photocatalysts with such a feedstock. The phoshides that we have begun investigating in objective 1 are suitable for photoelectrochemcial treatment of organics containing wastes.

Project Activities:

1) Discovery and optimization of potential photocatalytic materials

Summary of Accomplishments[1-6]

- Developed first and second generation automated electrochemical synthesis and screening systems.
- Explored the synthesis of doped Iron Oxide based materials systems.
- Investigated surface processing for optimal band edge position shift and electrocatalysis.
- Developed a spray pyrolysis synthesis system for hematite thin films with controlled Ti and Si doping.
- Designed and explored the synthesis of mesoporous and nanostructured delafossite and chalcogenide semiconductors.
- Developed a two-step route for the synthesis of transition metal phosphides.

The properties of the semiconductors investigated for this application, which are similar to those in photovoltaic devices, must satisfy conditions in several areas if cost-effective hydrogen production is to be realized: (1) efficient solar absorption, (2) effective charge separation/transport, (3) appropriate conduction band / valence band energies relative to H_2 and O_2 redox potentials ("band matching"), (4) facile interfacial charge transfer, (5) long-term stability, and (6) low cost. A material which satisfies all the above conditions simultaneously

could provide clean hydrogen in bulk and at low cost; unfortunately, no such material or system has been discovered or developed to date. The DOE has identified the following future targets for STH efficiency and durability: 2006, 4%; 2013, 8% and 1,000 hrs; 2018, 10% and 5,000 hrs.

Hematite (α-Fe_2O_3) has many potential advantages for hydrogen photoproduction. It has a bandgap of 2-2.2 eV (absorbs approximately 40% of the solar spectrum), it is stable in electrolytes over a wide range of pHs and is abundant, inexpensive and non toxic [1-3]. Several qualities have limited the use of this material as an efficient photocatalyst, including: i) high electrical resistance and high recombination rates of photogenerated electrons, and ii) a conduction surface band-edge that is lower than the redox level of H^+/H_2 [4-5]. The undesirable electrical properties are partially due to the hopping mechanism of charge transfer via oxygen vacancies, grain boundaries, and surface traps, which results in relatively low quantum yields. The low conduction band has been attributed to the Fe 3d electron configuration. Efforts have been devoted to reducing the resistivity of thin films by nanostructured crystal engineering. The electron transport resistance along the (001) planes of the hematite is 4 orders of magnitude lower than that in the direction perpendicular to this plane. By growing crystalline hematite nanorods oriented in the (001) direction, this anisotropic electron transport can be exploited to improve photocatalytic rates. Our hypothesis is that by deliberately doping hematite with selected heteroatoms [6] and being able to control the growth dimensions, crystal orientation and facets exposed, these limitations may be overcome. There is much diversity to explore in searching for the appropriate combination of dopant species to improve photocatalytic performance, [5, 8-10] as well as to understand and engineer the crystal structure, orientation and size of the crystalline domains of hematite. Another approach is to modify the surface reaction of semiconductors, through band edge shift, surface electrocatalyst deposition, and alternate polyalcohohl as electron donors, to further improve the performance of photocatalysis.

The approach involves the application of combinatorial chemistry methods to synthesize and optimize PEC materials and systems for cost-effective hydrogen production. This represents a systematic and high-speed exploration of new metal-oxide based solid-state materials. Our approach focuses upon the investigation of semiconductor materials that are inherently inexpensive, such as iron oxide. Iron oxide materials can be synthesized by rapid serial electrodeposition techniques or can be synthesized by sol-gel or spray pyrolysis, however, the limiting step in this case is still the high-throughput screening of materials, thus by utilizing the high-throughput screening system we can expedite the material discovery. By investigating large arrays of diverse doped hematite films, we are working to improve the understanding of the fundamental mechanisms and composition-structure-property relationships within these systems. Surface modification has been attempted to shift the flat band potential of doped hematite and to increase the zero bias photocurrent.

The automated electrochemical synthesis system has been designed and improved allowing using electrodeposition for a variety of new materials with program controls over electrochemical parameters like voltage, scan rate, cycle numbers, etc. The automated photoelectrochemical characterization system has been designed and constructed for the characterization of photocurrent, photovoltage, flat-band potential, incident photon conversion efficiency IPCE. The sketches of the high throughput electrochemical synthesis system and the automated photoelectrochemical characterization system are shown in Figure 1.

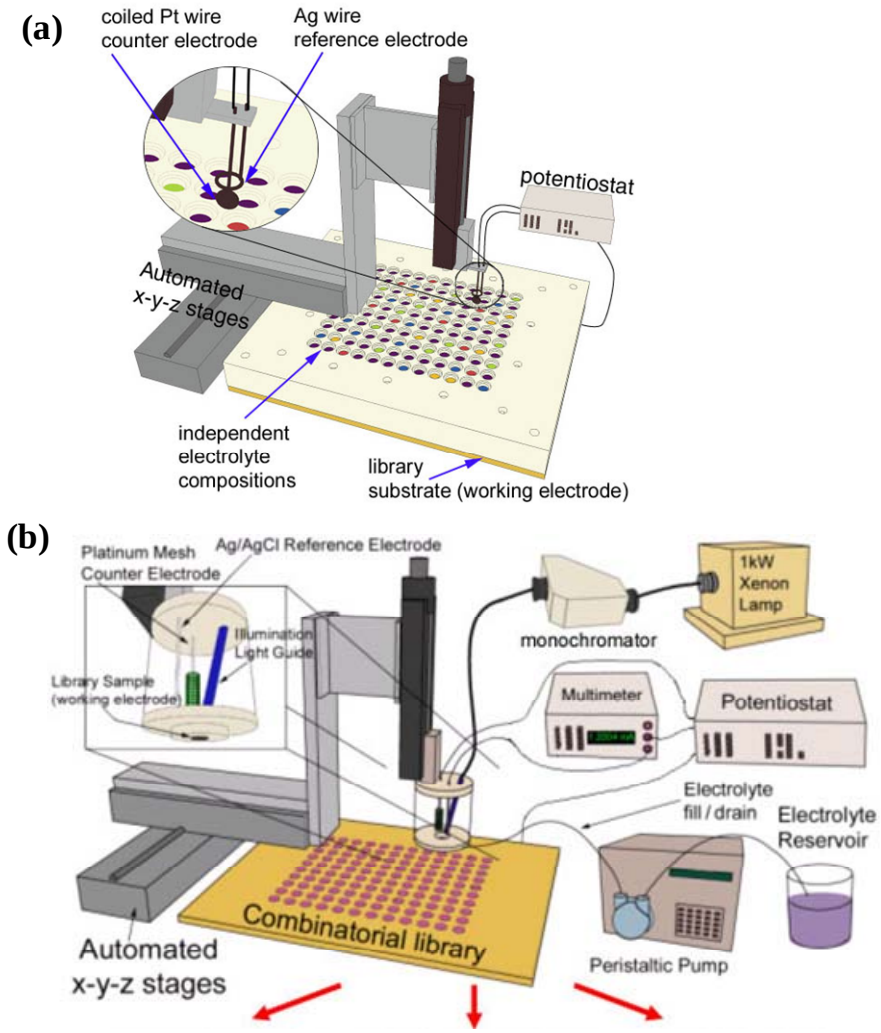

Figure 1. (a) Automated electrochemical synthesis system based on rapid-serial cyclic voltammogram deposition: 36 independent electrochemical cells are sealed upon a single conductive substrate. (b) Automated photoelectrochemical characterization system for photocurrent, photovoltage, flat-band potential, incident photon conversion efficiency IPCE characterization.

We have focused mainly on Fe_2O_3 host, investigating libraries of variable composition and structure. α-Fe_2O_3 thin films with different dopants have been synthesized by co-electrodeposition techniques. Around 30 dopants such as Al, Zn, Cu, Ni, Co, Cr, Mo, Ti, Pt, etc. were investigated. Doping with Al, Ti, Pt, Cr, and Mo exhibits the most promising results. Here we show the results of Cr, Mo, Pt, and Al doping in Figure 2.

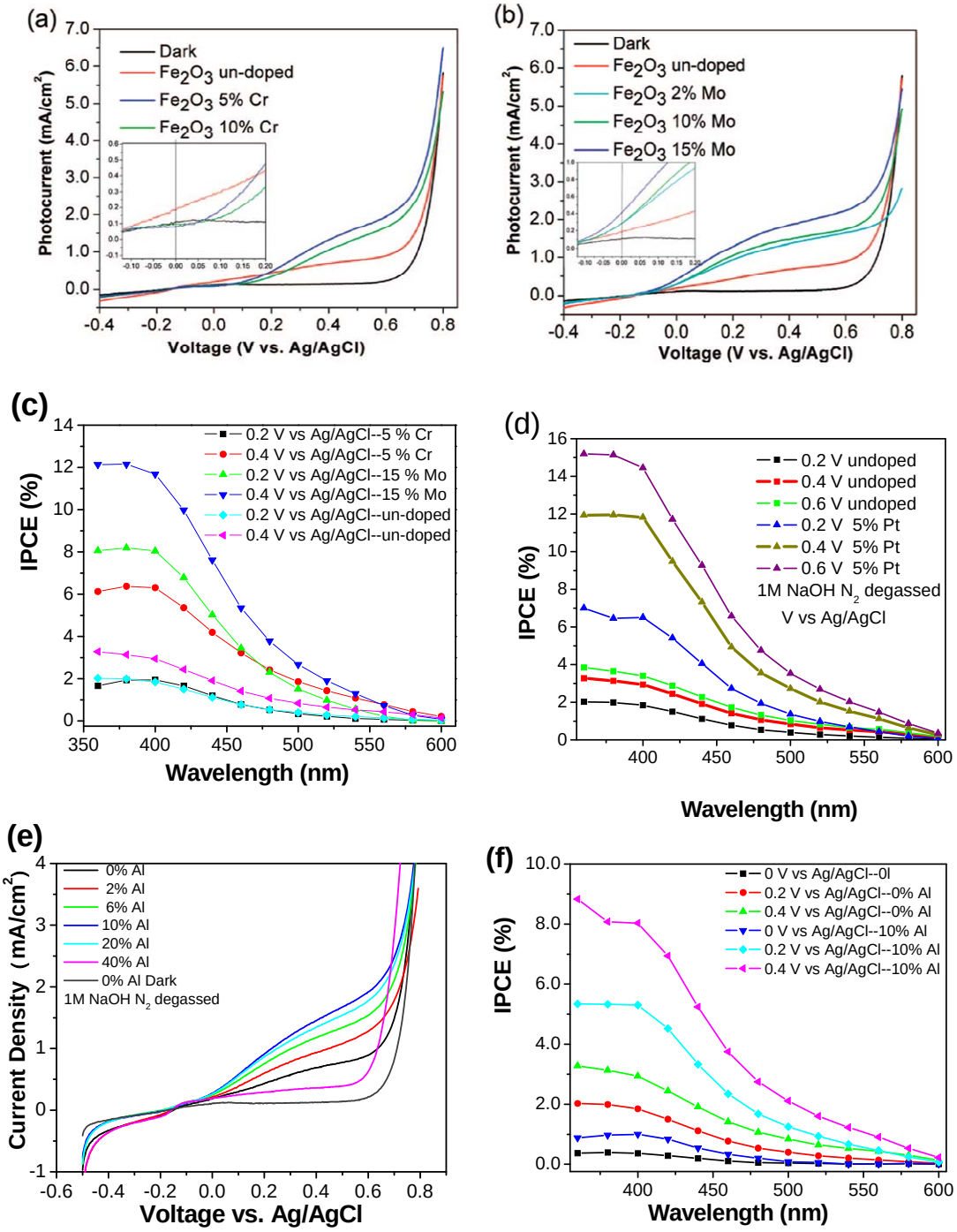

Figure 2. IV curves of (a) Cr doped and (b) Mo doped hematite at 410 mW/cm^2 illumination. Inset shows magnification of origin. (c) IPCE of the electrodeposited hematite films with and without doping (Cr, Mo) at different applied potentials in N_2 degassed 1 M NaOH. (d) IPCE of the electrodeposited hematite films with and without doping (Pt) at different applied potentials in N_2 degassed 1 M NaOH. (e) IV-Curves of the electrodeposited hematite films with and without doping (Al). (f) IPCE of the electrodeposited hematite films with and without doping (Al).

Besides their PEC performances, the phases, morphologies, optical properties and elemental components of the doped iron oxide thin films have been characterized by X-ray diffraction, scanning electron microscopy, ultraviolet-visual, and X-ray photoelectron spectroscopy, and Raman spectroscopy. Upon doping, the microstructures of the films varied; however, no preferred crystallographic orientation or dopant phase segregation was observed. There was only a small difference in the absorption properties of doped and undoped samples, which is mainly due to the variations in the sample thickness and morphologically dependent scattering of the films. Figure 2a, b and c show the photocurrent and incident photon conversion efficiency (IPCE) of Cr and Mo doped hematite thin films. Figure 2d shows IPCE of Pt doped hematite thin films. The best performing samples were 5% Pt and 15% Mo doped which had IPCEs at 400 nm of 12% at an applied potential of 0.4 V vs. Ag/AgCl. These IPCE values were 4× higher than the undoped sample for the 5% Pt and 15% Mo samples, respectively. The chopped current-voltage (IV) curves for Al doped iron oxide thin films, Figure 2e, show the best performance with 10% of Al in the electrolyte bath. The 10% Al in the electrolyte bath, which corresponds to a 0.3-0.5% doping, gives the IPCE at 400 nm of 8%. The increase in performance for Cr or Mo doped hematite thin films is attributed to an improvement in the charge transport properties within the films and not due to significant changes in the electrocatalytic rates due to dopants residing at the surface. Pt acts as an electron donor (substitution of Fe^{3+} by Pt^{4+}) in the hematite lattice and the increased donor concentration in the n-type doping would translate into an improvement in the conductivity and enhance charge transfer while decreasing carrier recombination. The increased donor concentration would increase the electric field across the space charge layer resulting in a higher charge separation efficiency. The higher PEC performance for Al doped hematite is believed to be due to the increased conductivity of the hematite associated with the strain introduced in the lattice from aluminum substitution of iron.

The doping of heteroatoms has been shown to increase the conductivity of hematite by orders of magnitude and thus the PEC performance on water splitting. However, the energy of the conduction band relative to the redox level of the H_2/H^+ couple is too low (~0.2 V vs. the normal hydrogen electrode) to efficiently drive the hydrogen evolution reaction. Therefore, all publications with hematite require an external bias to shift the conduction band position above the hydrogen evolution potential. We have demonstrated an effective way to shift the conduction band position of Ti doped hematite through surface modification using fluoride, which forms Ti-F bonds on surface. Figure 3 shows the improved PEC performance of Ti doped hematite thin films by CoF_3 (aqueous solution, pH~3.0) treatment. The CoF_3 treated samples show improvement in photocurrent at low bias (V <0.3 V vs. Ag/AgCl). The photocurrent onset potential for the treated sample is lower (~0.2 V) than the control sample. Furthermore, the untreated sample shows a negligible photocurrent at zero bias measured between the sample photoanode and the Pt mesh counter electrode without a reference electrode whereas a CoF_3 aqueous solution treated sample shows a photocurrent of approximately 150 $\mu A/cm^2$ under identical conditions and remains stable for more than 3,000 s (see Figure 3c). We propose that, the flat-band potential of the sample is more negatively shifted after CoF_3 treatment. This hypothesis is confirmed by the Mott-Schottky analysis, which shows a negative shift of ~0.15 V for the treated sample. When glucose was used as the electron donor, the photocurrent was further increased, as shown in Figures 3b, c and d, which is consistent with the slower rate for the oxygen evolution reaction of water oxidation than for the oxidation of glucose. The IPCE of

the fluoride treated sample with the presence of glucose at zero bias (only 2-electrode) reaches 3.7% at 400 nm with respect to 1.5% in the absence of glucose and 0.1% for control sample, Figure 3d.

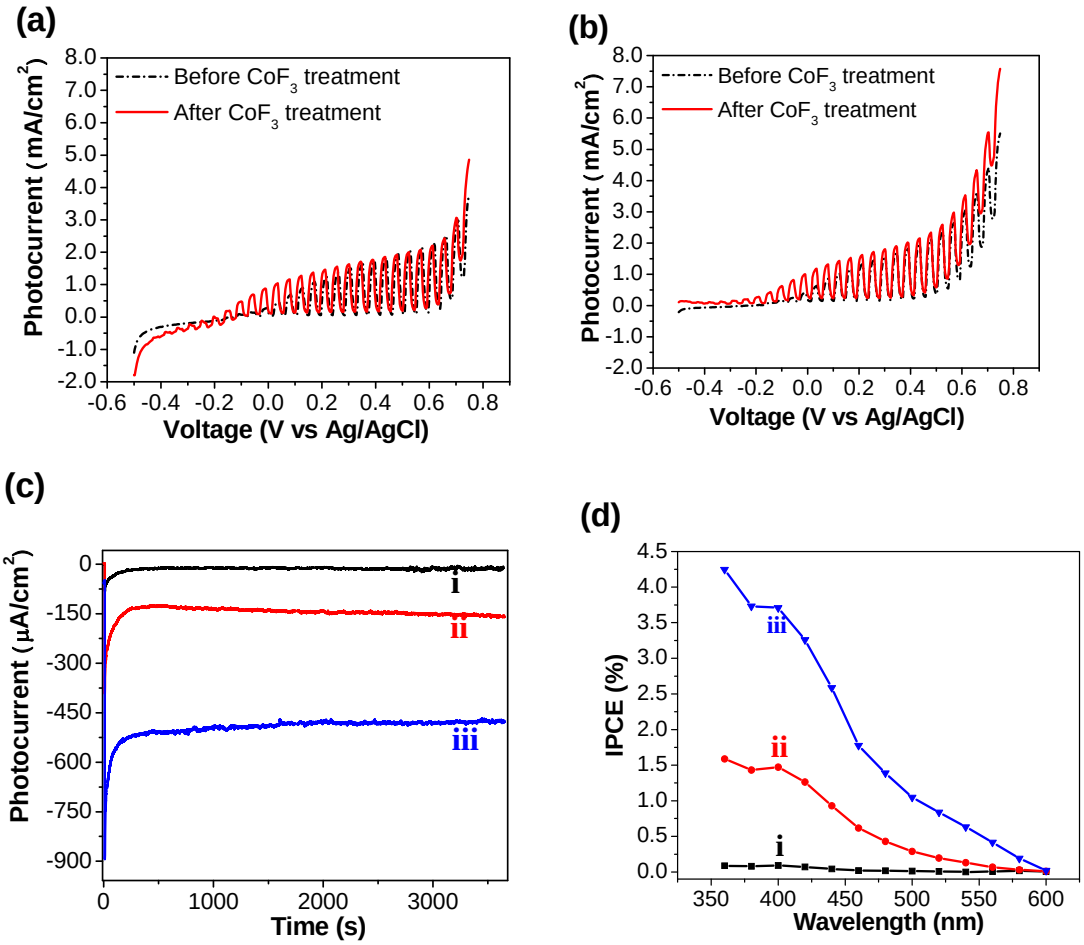

Figure 3. Chopped *I–V* curves of 6% Ti-doped iron oxide thin films before and after CoF_3 aqueous solution treatment in N_2 degassed 1 M NaOH solution (a) without glucose and (b) with 10 mM glucose; (c) zero bias photocurrent under white light illumination for the same samples: (i) before and (ii) after CoF_3 aqueous solution treatment, (iii) after CoF_3 aqueous solution treatment in the presence of glucose in the electrolyte; and (d) IPCE performance at zero bias (i, ii, iii are the same as in (c)).

We developed a microwave plasma reactor and reaction conditions for the synthesis of amorphous SiC nanoparticles in a continuous gas phase process are amenable to large scale production use. The process utilizes the decomposition of tetramethylsilane (TMS) for both the silicon and the carbon source. PEC performance of the materials was poor and oxidation in electrolyte irreversible and destructive.

Group III phosphide materials such as indium phosphide (InP) have been studied as photoelectrodes [11]. InP is highly active in hydrogen production with certain surface modifications [12]. However, indium is an expensive metal. Gallium phosphide (GaP) has excellent electrical properties, but its bandgap (2.24 eV @ 300K) is too wide to make a desirable semiconductor for optimal solar-to-chemical conversion efficiency. Bandgap engineering by doping is commonly used in III-IV compound semiconductors and our idea is to dope GaP with selected transition metals to narrow the bandgap. Transition metal phosphides, such as Ni_2P, WP, and MoP have narrow bandgaps [13]. The selection of these materials is due to their appropriate bandgap, and suitable positions of their conduction and valence bands. While the proper bandgap allows for absorption of a significant part of the visible spectrum, their appropriate band edge positions make a wide range of electrochemical reactions possible. Furthermore the widespread availability and low cost of both phosphorous and the metals is an advantage when considering a suitable material for potential large-scale deployment.

One of the detrimental electrochemical reactions occurring on the surface of phosphides is its cathodic decomposition resulting in formation of $M^0 + PH_3$ [14]. It is believed that surface modification can suppress these compositional changes and is the key for obtaining systems that are effective for long term operation. On the other hand, chemical reactions between the phosphides and chemical species such as halogens (e.g. Br_2) [15] undoubtedly necessitates implementation of some effective and viable surface passivation. In addition, tuning of the depletion width, and in fact the entire field that is built into both particle and wafer systems, as well as the quality of surface states deserve a great deal of attention in order to realize maximum efficiency.

The approach included (1) using InP as a model system to understand and improve its stability and photoelectrochemical performance in a number of commonly used active redox containing electrolytes. This result will allow for the selection of the best working conditions for synthesized transition metal phosphides in a particulate PEC system; (2) establishing simple methods for synthesizing phosphide materials; and (3) investigating alternative redox couples in which phosphides are stable for solar energy-to-chemical conversion. A slurry PEC reactor and hydrogen production measurement system was used for screening new photocatalyst materials.

A photoelectrochemical reaction and characterization system for colloidal photocatalysts was designed and applied for screening of new potential photocatalysts (Figure 4a).

(a)

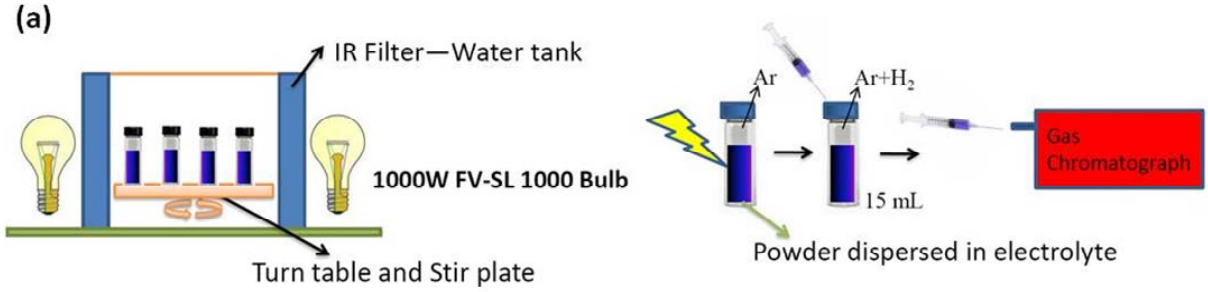

(b)

	Morphology	Electrolyte	Light source	H_2 (GC)
$CuCrO_2$	Mesoporous	NaOH+Na2S	visible	Y
$CuGaS_2$	Nanoparticle	NaOH+Na2S	visible	small
$CuLaO_2$	Nanoparticle	NaOH+Na_2S	visible	Y
$CuGaSe_2$	Mesoporous	NaOH+Na_2S	visible	Y
$CuGaSe_2$	Nanoparticle	NaOH+Na_2S	visible	N
WSe_2	Mesoporous	NaOH+Na_2S	visible	N
WO_3	Mesoporous	HBr	visible	small
InP	Particles	NaOH+Na_2S	visible	Y
$CuGaO_2$	Nanoparticle	NaOH+Na_2S	visible	Y
$CuCr_2O_4$	Mesoporous	NaOH+Na_2S	visible	Y

Figure 4. (a) Schematics of photoelectrochemical reactor and hydrogen production measurement system using gas chromatograph. The PEC reactor includes two 1,000 W bulbs and two water tanks as infrared filter. Nine sample vials can be held on the turn table in the metal box. Sample powders were dispersed in the vial and purged with Ar before illumination. After illumination, 500 µL gas sample was obtained from the headspace of the vial and injected into a gas chromatograph for hydrogen concentration analysis. (b) Screening results of semiconductors on hydrogen production under visible light illumination. The concentration of NaOH +Na_2S electrolyte is 1 M NaOH and 0.025 M Na_2S. The concentration of HBr electrolyte is 0.025 M.

Photocatalyst powders (~10 mg) were dispersed in 15 mL electrolyte and sealed by a septum in a 20 mL glass vial. The vials were illuminated in a PEC reactor by two 1,000 W light bulbs with infrared filters. The PEC reactors can hold nine vials and do a screening for them by injecting gas samples from headspace of the vials into gas chromatograph. This system has been applied in screening a variety of semiconductors (Figure 4b) in terms of their photoelectrocatalytic hydrogen production rate under visible light illumination. Several semiconductors have been shown to be active in hydrogen production under visible light illumination in basic Na_2S solution, such as $CuCrO_2$, $CuGaO_2$, $CuLaO_2$, $CuGaSe_2$, and InP.

Various surface treatments were explored to improve the corrosion resistance of phosphides. One method is to create sulphur bonds on the surface of the phosphide film or particles. Another treatment is the deposition of a metal as a cocatalyst to lower the kinetic barrier in solution. Sulfur surface treatment was tried on the tungsten phosphide colloidal. The

methods of Lim et al. [16] were used with only minor modifications. In our case powders are being processed instead of wafers, and dodacanethiol was used in place of octadecanethiol. The results of hydrogen evolution evaluation over 21 h are shown in Figure 6. The dark reaction is consistent between the two systems, but dodacanethiol allows much greater charge transfer to the solution as evidenced by the greatly improved H_2 evolution. Two metals, Rh and Ru, were photodeposited on tungsten phosphide. Both were deposited from an aqueous solution containing 50mg of the phosphide. The Rh solution contained 10% methanol as a sacrificial electron donor to complete a redox reaction and leave reduced metallic form of the metals on the surface. In both cases UV light was used for deposition. No significant catalytic effect is seen for either Rh or Ru (Figure 5).

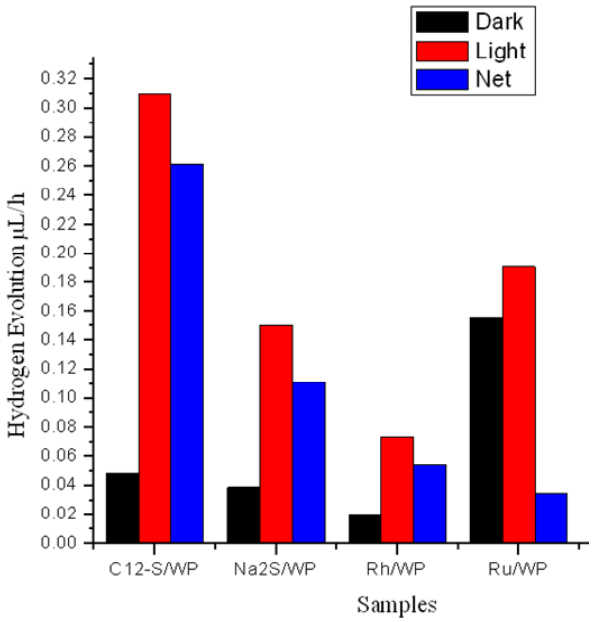

Figure 5. Hydrogen evolution (µL) from 200 mg WP powder samples under sunlight illumination for 21 hours in 15ml 0.1M HI/ DI H_2O solution measured using gas chromatography. As implied from the figure legend, the blue bars (Net) represent the difference between the dark and illuminated conditions.

Commercially available p-type InP wafers were used as photoelectrodes to investigate different redox couples (I^-/I_2 or I_3^-, Br^-/Br_2). A low resistance ohmic back contact, consisting of 30 nm Zn and 100 nm Au from electron beam deposition, was identified. The PEC performance of the p-InP wafer was studied with the Zn/Au ohmic back contact and surface deposited Pt nanoparticles as cocatalyst. Pt nanoparticles was deposited photo-electrochemically in a 1.6 mM H_2PtCl_6 aqueous solution by applying -0.35 V vs. Ag/AgCl while under illumination at 45 mW/cm^2 of white light. The deposited Pt particles of ~ 20 nm were uniformly dispersed on the surface (Figure 6a). Intensive hydrogen evolution from the InP wafer surface and simultaneous formation and precipitation of brown I_3^- from the back ohmic contact were detected in 0.5 M HI solution under 100 mW/cm^2 white light illumination. The efficient hydrogen production was confirmed by the IPCE and photocurrent measurements in a two-electrode configuration with zero bias. The IPCE of p-InP ($3x10^{16}$ doping density) in 0.5 M HI yields an average value of *ca.*

35% in a wide range of visible light from 500-900 nm, Figure 6b. A short-circuit photocurrent of 10 mA/cm^2 was also observed under 1 sun illumination. The effect of doping density (Zn as dopant) in p-InP on the overall hydrogen production performance was also investigated. Figure 6d shows the photocurrents of p-InP with three different doping densities, 3×10^{16}, $5\times10^{17}$and 5×10^{18}, in a two-electrode setup under 1 sun illumination. p-InP with the lowest doping density (3×10^{16}) exhibits the best performance. It is believed to be due to the wider depletion zone of this wafer which is more efficient in photo-generated electron/hole separation, as confirmed by the Mott-Schottky analysis results (Figure 6e). The valence band position of the p-InP was not positive enough to oxidize Br^- to Br_2. S-doped (2×10^{17}) InP which is essentially an n-type semiconductor was tested in 0.5 M HBr. The photocurrent under 100 mW/cm^2 of visible light illumination is shown in Figure 6f. Cyclic voltammetry experiments under illumination and dark indicated a photovoltage of *ca.* 0.8 V which is the difference between the redox potential of H^+/H_2 and Br^-/Br_2. Our preliminary results on the effect of pH, temperature, and concentration of HBr solution indicated that higher efficiencies (short circuit photocurrents) were obtained at lower pH, higher temperatures, and higher concentrations.

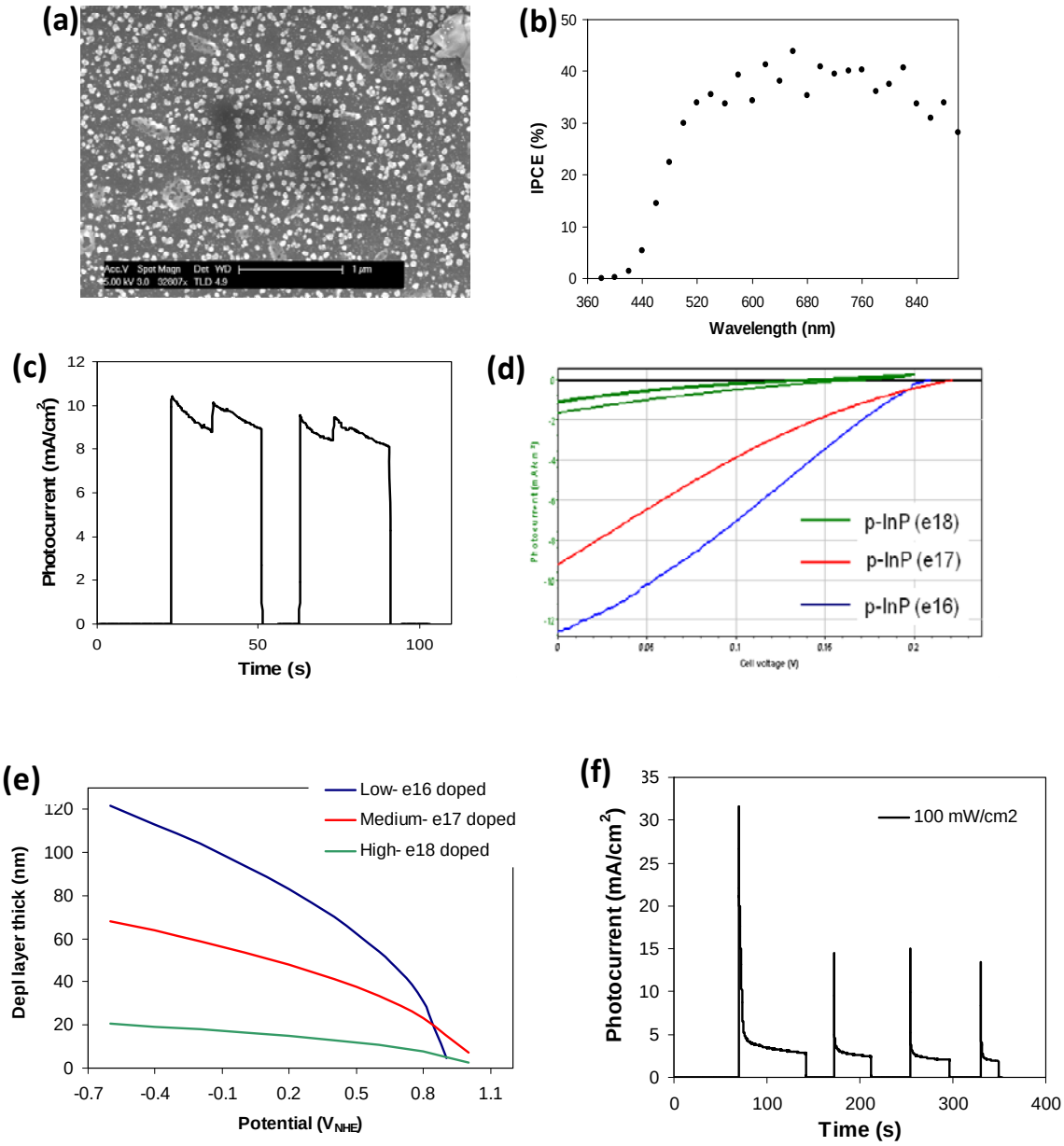

Figure 6. (a) SEM morphology of Pt nanoparticles deposited on InP surface by photoelectrochemical deposition. IPCE (b) and photocurrent (c) of $3X10^{16}$ p-InP wafer with Ohmic contact and surface Pt deposition in a 0.5 HI solution. The photocurrent in (b) was recorded under 100 mW/cm^2 illumination. (d) IV curves of p-InP with three different doping densities with photoelectrochemically deposited Pt and Au/Zn back contact in 0.5 M HI/$NaClO_4$. (e) Depletion layer thickness of p-InP with doping density of $3X10^{16}$, $5X10^{17}$ and $5X10^{18}$. A lower doping density corresponds to a thicker depletion layer with applied bias of lower than 0.85 V_{NHE}.

Several transition metal phosphides have been synthesized in our laboratory to date by a simple two-step route. The synthesis procedure includes the treatment of a metal or metal oxide with orthophosphoric acid at 500 ºC for *ca.* 24 h to form metal phosphate, followed by reduction in hydrogen at a higher temperature (550 – 950 ºC) for 6 – 48 h to the corresponding metal phosphide. This route has been applied to synthesize single phases of a number of semiconducting phosphides: MoP, WP, Ni_2P, and GaP. Solid solutions of $Ga_xMo_{1-x}P$ with Mo concentration up to 10% were synthesized.

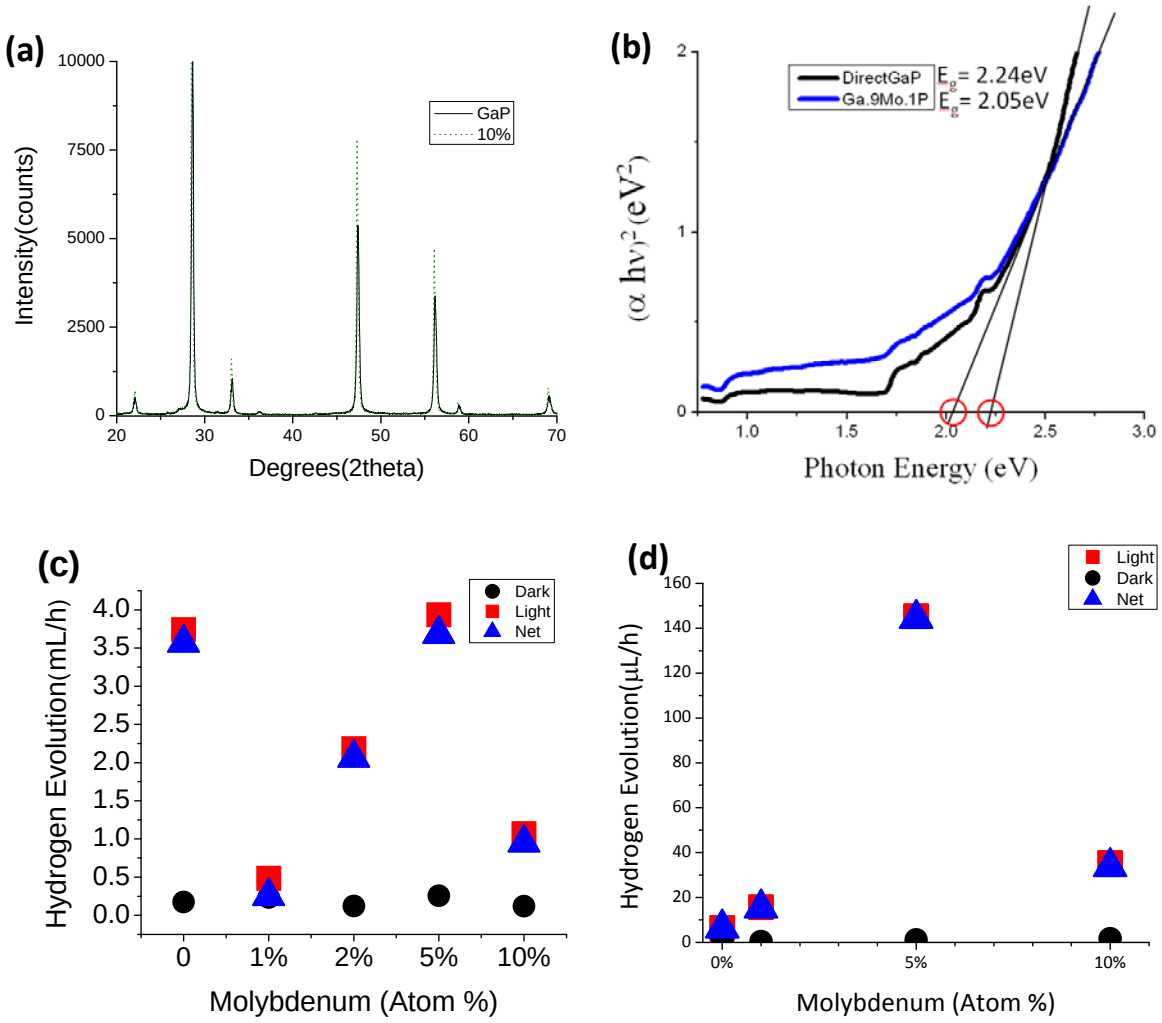

Figure 7. (a) XRD patterns of GaP and $Ga_{0.9}Mo_{0.1}P$ (nominal). (b) Tauc plots for GaP and $Ga_{0.9}Mo_{0.1}P$ derived from their UV-Vis spectra. Hydrogen evolution from closed vials containing 20mg samples of $Ga_{1-x}Mo_xP$ (c) with, (d) without Pt cocatalyst in 0.1 M HI continuously illuminated over 24 h.

Figure 7a shows the XRD patterns of GaP and $Ga_{0.9}Mo_{0.1}P$ (nominal) and the reflection lines overlay with each other. The Taut plots from UV-Vis spectra for GaP and $Ga_{0.9}Mo_{0.1}P$ (nominal) (Figure 7b) show a noticeable decrease in the bandgap upon 10% Mo doping. The hydrogen evolution evaluation results for $Ga_xMo_{1-x}P$ with and without surface deposited Pt nanoparticles are shown in Figure 7c, and 7d. 5% Mo doped sample exhibits the best hydrogen evolution performance. Deposition of Pt cocatalyst improves hydrogen production dramatically.

2) Optimizing the nanostructure of the material for maximum efficiency

Summary of Accomplishments[7-11]

- Development of synthesis conditions for the synthesis of Iron oxide nanorods with control over the feature size of the nanorods.
- Explored the synthesis of mesoporous Iron Oxide by a template method.
- Designed and explore the synthesis of mesoporous and nanostructured delafossite and chalcogenide semiconductors.

Our objective was to develop combinations of absorbers and electrocatalysts which provided efficient transfer of photogenerated electrons and holes to produce hydrogen and oxygen. A three-step method was employed to synthesize monodispersed silica encapsulated composite nanostructures with Pt nanoclusters (<1 nm) densely deposited on the surface of core hematite nanocubes. In addition, we developed nanocomposite magnetite cores with silica shells. Electrocatalytic metals were produced including gold-platinum (Au-Pt) clusters synthesized by electrodeposition. A nickel iron binary oxide electrocatalysts prepared from different precursors were evaluated to facilitate the oxygen evolution reaction (OER) on photoelectrodes and their activities characterized. The kinetics of electrocatalytic oxygen reduction in basic electrolyte on Au nanoparticles was also determined for 3 and 7 nm clusters supported on carbon. Finally, the electroreduction of oxygen was investigated on mixed gold-cobalt oxide (Au/CoO_x) nanoclusters in potassium hydroxide solution. The Au/CoO_x binary electrocatalysts with less than 1.2% Co atoms were found to increase the ORR activity compared to those of either the pure Au or pure CoO_x.

The effect of oriented growth of hematite and dopant concentration on the photoactivity of Ti doped hematite thin films were investigated by atmosphere pressure chemical vapor deposition (APCVD) from anhydrous precursors, Figure 8a.

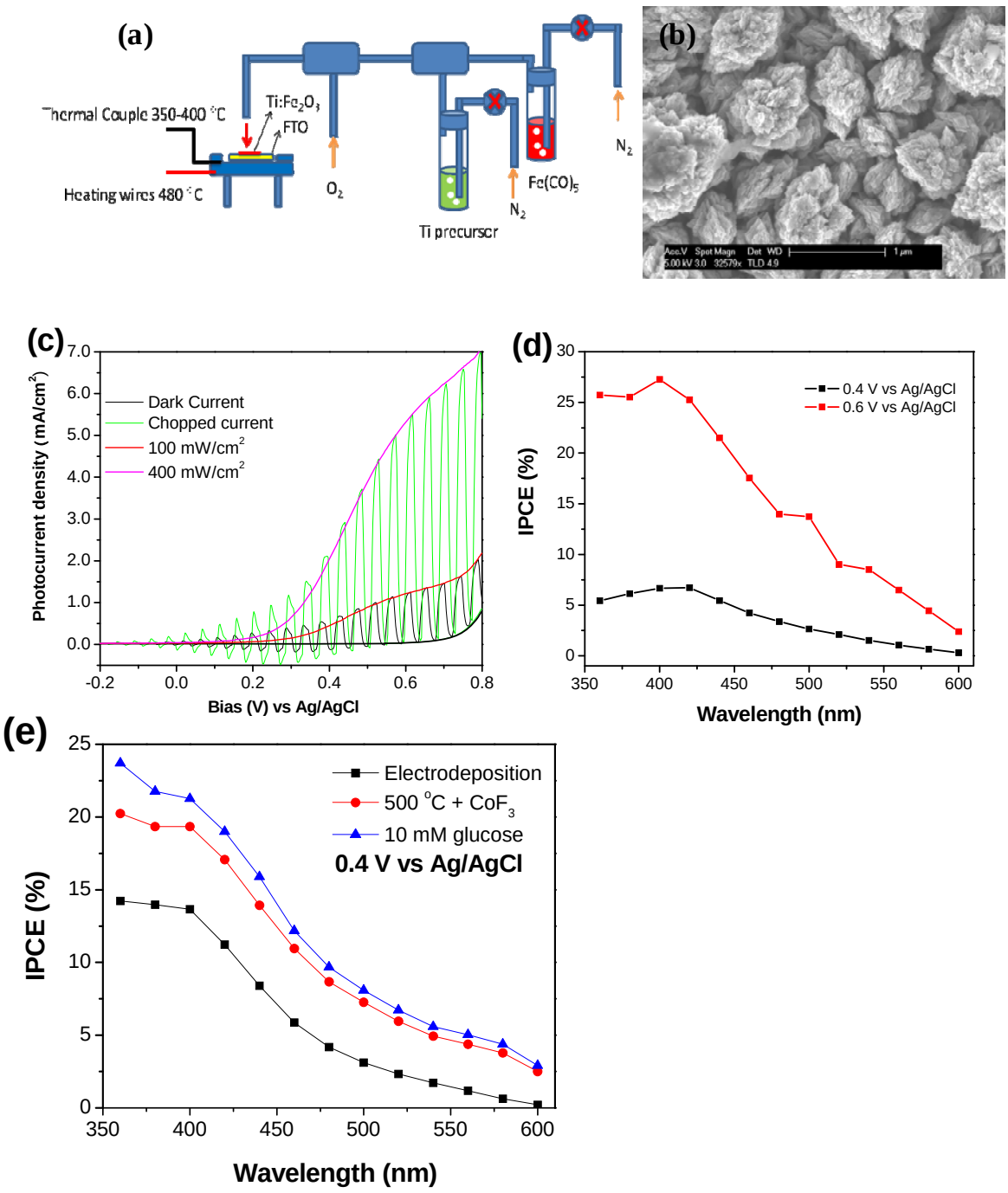

Figure 8. (a) Schematics of atmosphere pressure chemical vapor deposition (spray pyrolysis) method for preparation of Ti doped hematite thin films; (b) scanning electron microsope image of Ti:Fe_2O_3 thin film sample with 0.8% Ti doping. (c) 3-electrode chopped IV curves for 0.8% Ti:Fe_2O_3 sample under 100 and 400 mW/cm^2 visible light illumination and N_2 degassed 1 M NaOH at a scan rate of 100 mV/s; (d) IPCE of the sample in N_2 degassed 1 M NaOH with 0.4 and 0.6V applied bias *vs.* Ag/AgCl. (e) IPCE of the sample after 500 °C calcination and CoF_3 treatment in 1 M NaOH, 1M NaOH and 10 mM Glucose, and sample prepared by electrodeposition in 1 M NaOH under an applied bias of 0.4 V vs. Ag/AgCl.

Using iron pentacarbonyl $Fe(CO)_5$ and titanium tetrachloride $TiCl_4$ precursors, faceted nanoparticles with sizes of 20-50 nm were obtained on the fluorine-doped tin oxide (FTO) glass substrates (Figure 8b). All hematite films deposited by APCVD show a (110) oriented growth. Ti doping changes the microstructure of the films significantly and dopant concentration affects the photoelectrochemical performance of the films, with the maximum of photoelectrochemical conversion efficiency at 0.8% Ti doping. Increasing Ti concentration results in an increase of particle size and lower IPCE. For the sample with 0.8% Ti doping, photocurrents of 1.2 and 5.3 mA/cm^2 were observed at 0.6 V vs. Ag/AgCl under visible light illumination of 100, and 400 mW/cm^2, respectively (Figure 8c). The IPCE of this sample approaches 6% and 27% at 400 nm with an applied bias of 0.4 V and 0.6 V vs. Ag/AgCl, respectively, Figure 8d. The onset potential for photocurrent is relatively high, (approximately -0.2 V vs. Ag/AgCl) and calcination at 500 ºC lowers the onset potential due to the decrease of the trap state density. Surface modification by CoF_3 improves further the photoelectrochemical performance with a photocurrent of ~100 $\mu A/cm^2$ at zero bias (two-electrode configuration) after surface modification. The IPCE at 400 nm is increased by a factor of 3 at 0.4 V vs. Ag/AgCl after calcination and surface modification, and is ~ 30% higher than Ti doped Fe_2O_3 samples prepared by electrodeposition described in the previous section (Fig 8e).

Electron beam (e-beam) vapor deposition was employed to produce an "ideal" α-Fe_2O_3 thin film with respect to stoichiometry, spatial homogeneity over cm^2, minimal contamination by impurities, minimal surface roughness, minimal nanostructuring, minimal "pinholes", and ultimately high reproducibility of the aforementioned ideality. Our standard substrate is a polished quartz wafer onto which 50 nm of Ti followed by 150 nm of Pt are e-beam deposited. Using this Q/Ti/Pt substrate without further treatment, Fe is then e-beam evaporated to the desired thickness. After deposition, the Q/Ti/Pt/Fe films are then cut into pieces of *ca.* 1x2 cm^2, and calcined in air at 700 °C for 4 hrs to oxidize Fe to Fe_2O_3. Here we present the results for 500 nm Fe thickness samples. The photocurrent onset (seen at -0.2 V vs. Ag/AgCl, Figure 9a) is observed at potentials 0.1-0.4 V more negative than the onset of many other published hematite films. This large improvement in open circuit potential (V_{oc}) may result from a dense, pinhole free film with a high shunt resistance and reduced surface trap state density. Flat band potential (V_{fb}) of the e-beam deposited α-Fe_2O_3 thin film was measured using AC impedance spectroscopy and its variation with pH is shown in Figure 9b.

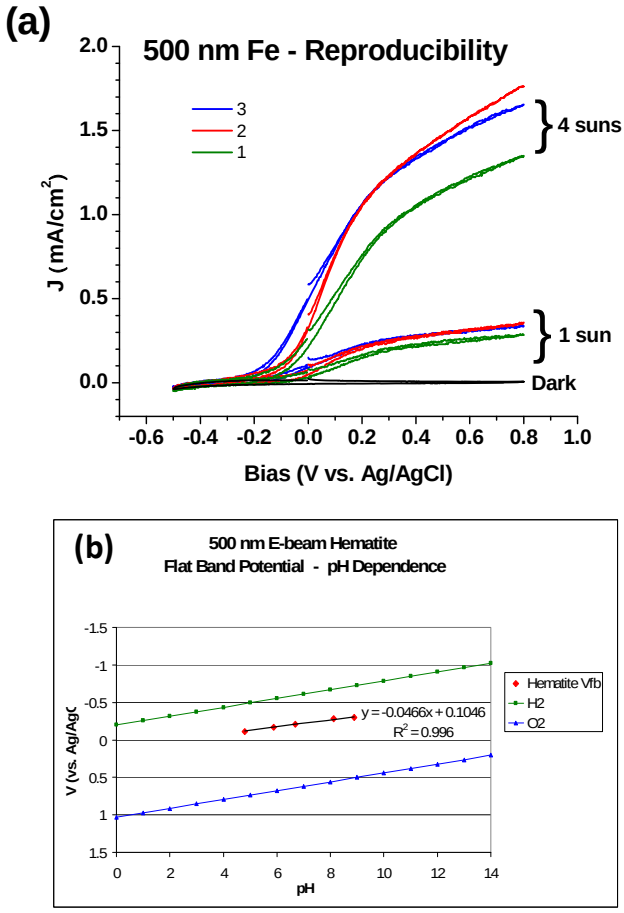

Figure 9. (a) IV curves of three identically fabricated hematite films tested in the dark, under 1 and 4 suns of illumination (100 and 400 mW/cm^2, respectively) in 1.0 M NaOH. (b) Flat band potential for hematite film in the dark. Data collected from fitting Mott-Schottky plots at each pH.

Accordng to the measurement in 0.5 M phosphate buffer at pH 7, hematite needs more than 0.4 V of external bias to spontaneously split water. A slope of -0.047 V/pH from our measurement indicates a non-Nernstian activity (-0.059 V/pH) of the film surface.

3) Create a conceptual large-scale reactor system in which a PEC material might realistically be used for producing hydrogen

Summary of Accomplishments

- Collaboration with colleagues at Directed Technologies to develop a photoelectrochemical process economic model.

- Explored the effect of poly-alcohols as alternate organic electron donors.
- Developed a photoelectrochemical reactor and hydrogen production measurement system for colloidal photocatalysts.

In collaboration with colleagues at Directed Technologies we participated in the development of a photoelectrochemical process economic model which showed that the most promising potential system design for cost effective hydrogen production is based on a slurry phase reactor design. We extended this model to examine a process for the conversion of organic wastewater associated with biofuel production as a source of oxidation potential for hydrogen production. Preliminary studies showed that significantly improved conversion efficiencies for hydrogen production were possible even for metal oxides (hematite) photocatalysts with such a feedstock. The phoshides that we have begun investigating in objective 1 are suitable for photoelectrochemcial treatment of organics containing wastes.

Our preliminary data indicates that even hematite (iron oxide) which has many challenges as a photocatalytic material for water splitting has a relatively high efficiency for hydrogen production when organics are used as electron donors. Figure 10 shows our preliminary data from a hematite photoelectrode that under one sun illumination and no applied bias with incident photon to electron conversion efficiency jumping from below 1% to over 10% at 1000 W/m^2 450nm illumination when the electron donor is changed from water to polyol analogs of wastewater.

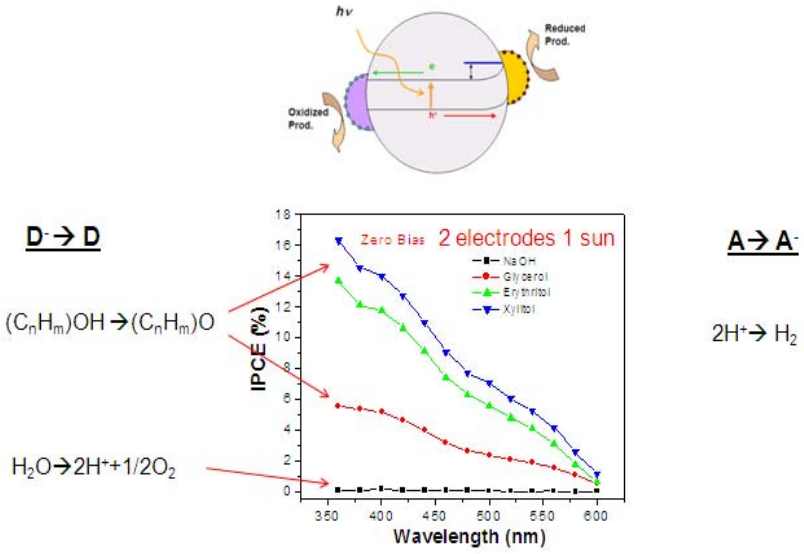

Figure 10. Schematic of photoelectrochemical reaction on a semiconductor particle, and IPCE of a hematite photoelectrode in basic electrolyte with organics.

Other investigators have investigated organic compounds as electron donors for hydrogen production including alcohols, organic acids, glucose, starch, as well as common organic pollutants. Levels of organics typical of municipal wastewater (250 - 1000 mg/l) as well as industrial wastewaters: (200 - 350,000 mg/l) have been investigated.

A final problem with water splitting is that hydrogen is an expensive molecule to store and transport. Our proposal includes a conceptual process modeling of a unique proposal for storage and transport of PEC produced hydrogen as methane in our natural gas pipeline system. We have developed low temperature and low pressure heterogeneous catalysts that are active for hydrogenation of carbon dioxide with a very high selectivity to methane. The PEC generated hydrogen will be combined with carbon dioxide in a gas phase thermal reactor at the PEC facility and the methane produced immediately

offloaded into the gas pipeline system. With over 1.9 million miles of distribution pipes and mains along with 300,000 miles of transmission pipelines this extensive infrastructure can serve as a critical element to a distributed renewable energy system.

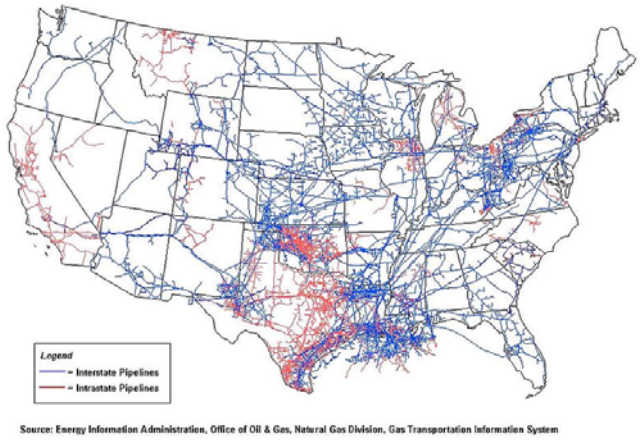

There is an additional 4,091 Bcf of natural gas storage facilities connected to this pipeline system. Few people realize that the U.S. has nearly 150 $x10^{21}$ Joules of energy storage capacity already existing and connected to almost every house and business in the country. Our total energy usage in the US is approximately 3.4 Terawatts (3.4 $x10^{12}$ Joules/s) and with only a tiny change in the system pressures tremendous energy storage capacity exists. This process scheme will eliminate all of the thus far insurmountable hydrogen storage problems associated with the cyclical production of hydrogen in solar facilities.

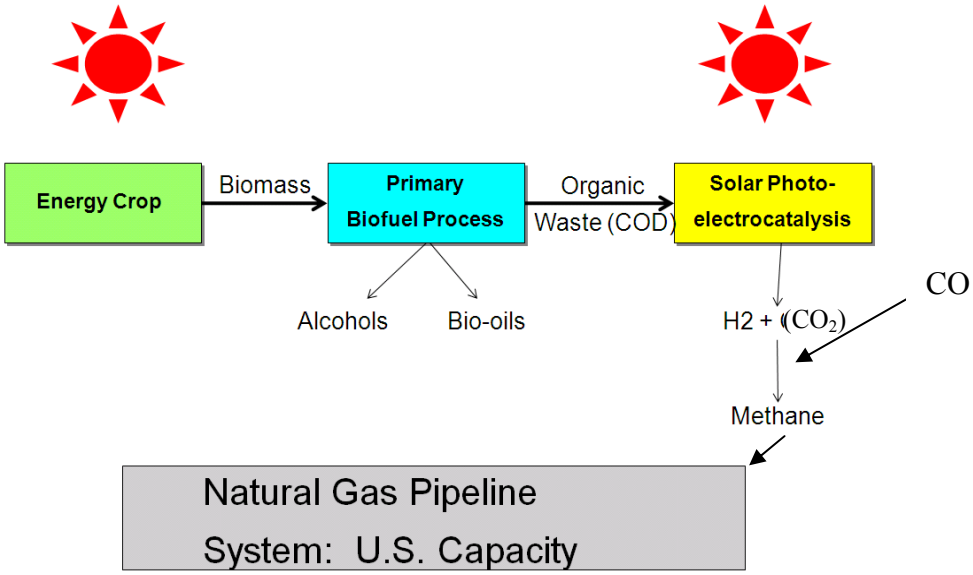

Natural gas utilities have been delivering natural gas for decades, some for more than a century thus the extraction of energy from this storage grid is time-tested. Further, it has been shown in India and South America that any gasoline powered car can be converted at minimal expense to run on compressed natural gas or in a flex fuel mode with user options to switch between the two.

We would make use of the waste stream from the developing infrastructure of biofuels in the U.S. Already corn ethanol facilities have significant organic loads in their wastewater with organic loading in excess of 100 mg/liter and the proposed biodiesel and algal bio-oil facilities extract less than 40% of the organics from their feed and discharge the remainder. These feedstock sources have low, if not negative, values which will be investigated as part of our conceptual process modeling activities.

Patents: No patents have been filed.

Recent Publications Crediting the DOE Hydrogen Program:

(1) Kleiman-Shwarsctein, A.; Huda, M. N.; Walsh, A.; Yan, Y. F.; Stucky, G. D.; Hu, Y. S.; Al-Jassim, M. M.; McFarland, E. W. *Chemistry of Materials* **2010**, *22*, 510.
(2) Chen, Z. B.; Jaramillo, T. F.; Deutsch, T. G.; Kleiman-Shwarsctein, A.; Forman, A. J.; Gaillard, N.; Garland, R.; Takanabe, K.; Heske, C.; Sunkara, M.; McFarland, E. W.; Domen, K.; Miller, E. L.; Turner, J. A.; Dinh, H. N. *Journal of Materials Research* **2010**, *25*, 3.
(3) Hu, Y. S.; Kleiman-Shwarsctein, A.; Stucky, G. D.; McFarland, E. W. *Chemical Communications* **2009**, 2652.
(4) Lin, H. F.; Gerbec, J. A.; Sushchikh, M.; McFarland, E. W. *Nanotechnology* **2008**, *19*.
(5) Kleiman-Shwarsctein, A.; Hu, Y. S.; Forman, A. J.; Stucky, G. D.; McFarland, E. W. *Journal of Physical Chemistry C* **2008**, *112*, 15900.
(6) Hu, Y. S.; Kleiman-Shwarsctein, A.; Forman, A. J.; Hazen, D.; Park, J. N.; McFarland, E. W. *Chemistry of Materials* **2008**, *20*, 3803.
(7) Zhang, P.; Chi, M. F.; Sharma, S.; McFarland, E. *Journal of Materials Chemistry* **2010**, *20*, 2013.
(8) Park, J. N.; Zhang, P.; Hu, Y. S.; McFarland, E. *Nanotechnology* **2010**, *21*.
(9) Tang, W.; Jayaraman, S.; Jaramillo, T. F.; Stucky, G. D.; McFarland, E. W. *Journal of Physical Chemistry C* **2009**, *113*, 5014.
(10) Kleiman-Shwarsctein, A.; Hu, Y. S.; Stucky, G. D.; McFarland, E. W. *Electrochemistry Communications* **2009**, *11*, 1150.
(11) Tang, W.; Lin, H. F.; Kleiman-Shwarsctein, A.; Stucky, G. D.; McFarland, E. W. *Journal of Physical Chemistry C* **2008**, *112*, 10515.

12. P. Zhang, "*Nanostructured Cu(X)O_2 Delafossite Photoelectrocatalysts for Solar-to-Chemical Energy Conversion"*, Talk, Presented at Materials Research Society, April 2009.
13. E. W. McFarland, "PEC Hydrogen Production", Invited tutorial, ECS Annual Meeting, June 2008.
14. E.W. McFarland. "PEC Production of Fuels and Chemicals", UCSB Symposium on Frontiers of Surface Science, June 2008.
15. E. W. McFarland, "*Design and Synthesis of Optimized Material Systems and Structures for Photoelectrocatalytic Production of Chemicals and Fuels From Sunlight*", Invited talk, 5th University of California Symposium on Surface Science and ITS Application, California, June 2008.
16. A. J. Forman, "*Multi-Component Nanostructured Semiconductors for Photoelectrocatalysis - Progress Towards Efficient and Stable Solar-to-Chemical Energy Conversion*", Oral presentation, Presented at Materials Research Society, March 24-28th, 2008.
17. A. Kleiman-Shwarsctein, "*Solar Hydrogen Production by Photo-oxidation of Water and Biomass with Hematite Nanorod Photoelectrocatalysts*" Poster, Presented at Materials Research Society, March 24-28th, 2008.

18. E. W. McFarland, "Nanostructured Photoreactors", Invited talk, Chalmers University, March 2008.
19. E. W. McFarland, "New Materials for PEC", Invited talk, Danish Technical University, July 2007.

Other References

[1] Khan S. U. M., A. J., *J. Phys. Chem. B*, 1999, **103**, 7184
[2] Bjorskten U, Moser J, Gratzel M, *Chem. Mater*, 1994, **6**, 858
[3] Beermann N., Vayssieres L., Linquist E. S., Hagfeldt A., *J. Electrochem. Soc.*, 2002, **147**, 2456
[4] Ahmed S.M., Leduc J, Haller S.F., *J. Phys. Chem. B*, 1988, **92**, 6655
[5] Arutyunyan V.M., Arakelyan V.M., Sarkisyan A.G., Shakhnazaryan G.E., Stepanyan G.M., Turner J. A, *Russ. J. Electrochem.*, 1998, **38**, 854
[6] Vayssieres L., Beermann N., Lindquist S E, Hagfeldt A, *Chem. Mater.*, 2001, **13**, 233
[7] Kay A, Cesar I, and Grätzel M, *J. Am. Chem. Soc.*, 2006, **128**, 15714
[8] Berry J. F., Greaves C., Helgason O., McManus J., *J. Mater. Chem.*, 1999, **9**, 223
[9] Prasad N. V, Srinivas K, Kumar S. G., J. A.R., *Appl. Phys. A*, 2001, **72**, 341
[10] Aroutuaunian V.M., Arakelyan V.M., Shahnazaryan G.E., Stepanyan G.M., Turner J. A., Khaselev O, *Int. J. Hydrogen Energ.*, 2002, **27**, 33
[11] Szklarczykt M. and Bockris J. O., *J. Phys. Chem.* 1984**, 88**, 5241
[12] Goodman C. E., Wessels B. W., and Ang P. G. P., *Appl. Phys. Lett.*, 1984, **45**,442
[13] Sharon M., Tamizhmani G., *J. Mater. Sci.*, 1986, **21**, 2193
[14] Lewerenz H. J., and Schulte K. H., *Electrochimica Acta*, 2002, **47**, 2639
[15] Parker R., Hydrogen-Based Utility Energy Storage System, Proceedings of the 2001 DOE Hydrogen Program Review NREL/CP-570-30535
[16] Lim, H., Carraro, C., Maboudian, R., *Langmuir*, 2004, **20**, 743